# 静電浮遊法を用いた高温融体粘性係数測定

○石川 毅彦，岡田 純平（宇宙航空研究開発機構），渡邊 勇基（エイ・イー・エス）

# Viscosity Measurement of High Temperature Melts using an Electrostatic Levitation Method

○Takehiko ISHIKAWA, Junpei OKADA (JAXA), Yuki WATANEBE (AES Co., Ltd.)

## 1. Introduction

In the recent decade, levitation techniques have made a substantial progress and have been utilized for many researches in materials science. Levitation methods enable containerless sample processing, with which problems associated with crucibles (i.e. contamination from crucibles or chemical reaction between samples and container walls) can be minimized. Moreover, since nucleation from the crucibles is suppressed, liquid samples can be brought to deeply undercooled temperatures. Levitation methods are widely used for thermophysical property measurements of high temperature melts. Density, heat capacity, emissivity, thermal conductivity, electrical resistivity, surface tension, and viscosity have been measured with several kinds of levitators. Viscosity has been measured by the drop oscillation method with both electromagnetic and electrostatic levitators. In this technique, a levitated melt is deformed from its spherical shape with an external electric field superimposed on the levitation field to excite drop oscillation. After stopping the excitation, the amplitude of sample oscillation decays due to its viscosity. Knowing the density of the sample ($\rho$), its radius ($R_0$), the viscosity ($\eta$) can be obtained from the measured decay time ($\tau$) and the following formula:

$$\eta = \frac{\rho R_0^2}{5\tau} \quad (1)$$

The Viscosities of refractory metals over 2000 K have been successfully measured by this method. However, drop oscillation method is not applicable for highly viscous samples such as bulk metallic glass (BMG) alloys, since the drop oscillation is hard, if not impossible, to excite.

An alternative method to measure the viscosity on an electrostatically levitated sample has been proposed by Abe et al.,[1] using sample rotation. In this method, a levitated sample is spun with vertical axis. When the rotation ratio excesses a critical value, the sample shape transformed from axisymmetric to non-axisymmetric. If the sample is spun more, the sample shape becomes a dumbbells shape and finally breaks into two pieces. Abe et al. measured the terminal value of the maximum sample length and determine the viscosity. They have experimentally proved this technique using propylene carbonate, glycerol, and mixture of glycerol and glucose; all the samples are liquid at room temperature. However, there are a few difficulties to apply this technique for high temperature melts, including temperature homogeneity and experimental repeatability.

Another method proposed by Ohsaka et al.[2] also utilizes the sample rotation. After spinning the levitated sample beyond its bifurcation, they suddenly remove the rotation torque. Since the sample is levitated in gaseous atmosphere, the sample rotation stops quickly. Then the shape of viscous sample gradually returns from the dumbbells shape to sphere. They observe this shape change as a function of time and determine the viscosity. This technique can not apply to high temperature metals since a vacuum condition is required to prevent oxidization.

A new method currently studied in this paper also use sample rotation and bifurcation phenomena. In this study, a high speed camera is equipped to observe the transformation from axisymmetric to non-axisymmetric shape in high vacuum environment. This paper briefly describes the experimental setup, analysis, and results of preparatory experiments.

## 2. Experimental Setup

### 2.1 Electrostatic Levitator

The electrostatic levitation system used in this study is similar to the one developed by Rhim *et al.* [3] but includes several modifications. A detailed description of the facility is given elsewhere.[4] It consists of a stainless steel chamber that is evacuated to a pressure of around $10^{-5}$ Pa. The chamber (Fig. 1) houses a pair of parallel disk electrodes, typically 10 mm apart between which a positively charged sample is levitated using Coulomb force. These electrodes are utilized to control the vertical position of the specimen, which has a typical diameter of about 2 mm. In order to levitate the sample against gravity, a huge electric field of around 10 to 20 kV/cm is applied between these electrodes. In addition, four spherical electrodes distributed around the bottom electrode are used for horizontal control. High speed feedback control is necessary to maintain stable sample levitation.

The levitated sample is heated by high power $CO_2$ lasers, and the sample temperature is measured by single color pyrometers.

The lower electrode is surrounded by four coils. These coils create a horizontal rotating magnetic field that rotates at 400 Hz around the vertical direction. The principle of the sample rotation mechanism is the same as that of the asynchronous induction motor. The four coils act as a stator while the levitated sample serves as a rotor. The direction of the induced torque on the sample can be controlled by selecting the direction of the rotating magnetic field. Detailed explanation on this sample rotation mechanism is found in elsewhere[5].

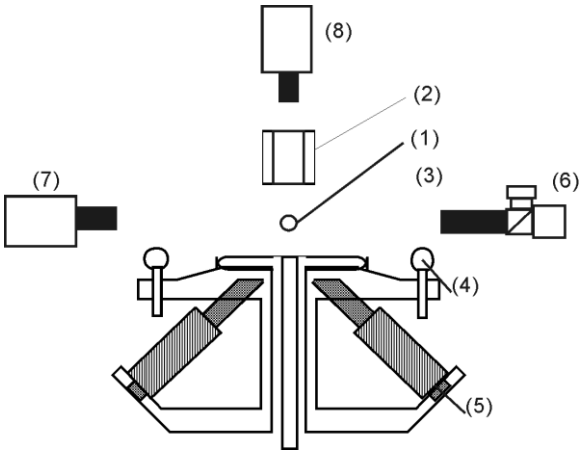


**Fig. 1** Schematic side view of the electrode assembly and observation system; (1) sample, (2) top electrode, (3) bottom electrode, (4) four side electrodes, (5) four coils, (6) rotation measurement system, (7) side view camera, and (8) high speed camera.

An observation camera, equipped with a telephoto objective in conjunction with a background UV lamp, provides a magnified side view of the sample. A rotation measurement system described later is also used. In addition, a high speed video camera (HSV) is set above the top electrode so that the sample rotation can be observed via the through the hole of the top electrode (Fig.1).

### 2.2 Analysis

After stable levitation is achieved, deliberate sample rotation in induced, and the levitated drop starts rotating around the vertical axis, its initial spherical shape changing to an oblate shape due to the centrifugal force. When the sample rotation frequency reaches a critical value ($\Omega_c$), the sample shape drastically changes from axisymmetric to non-axisymmetric (Fig.2). This change of shape is called bifurcation. The high speed camera recorded the sample shape around the bifurcation at 3000 fps for about 25 s. After the experiment, these images are analyzed with homemade software. In this software, aspect ratio (ratio between maximum and minimum length of drop radius) and the angle of maximum radius ($\phi$; definition given in Fig. 2(b)) were determined. From the analyses of more than 70000 images, the data array of $\phi$ as a function of time was created, from which the rotation frequency and was calculated.

## 3. Experiment and Result

A zirconium (whose viscosity is about 4 mPa·s) and a glass forming alloy (ZrCoAl; whose viscosity is about 40 mPa·s) were selected for the preliminary experiment. Each sample was levitated, molten, and spun. Figure 3 shows the change of aspect ratio after the bifurcation, It is noticed that in the viscosity of the sample may affect the speed of shape transformation from axisymmetric to non-axisymmetric. Further experiments with a variety of samples are necessary to get secure conclusions.

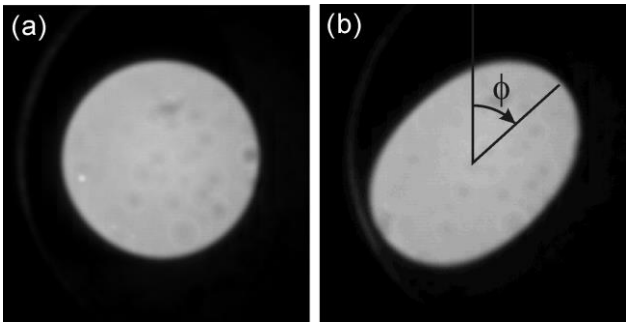


**Fig. 2** Sample images taken by the high speed camera through a hole in the top electrode; (a) axisymmetric, and (b) non-axisymmetric. $\phi$ indicates the rotation angle measured by image analysis.

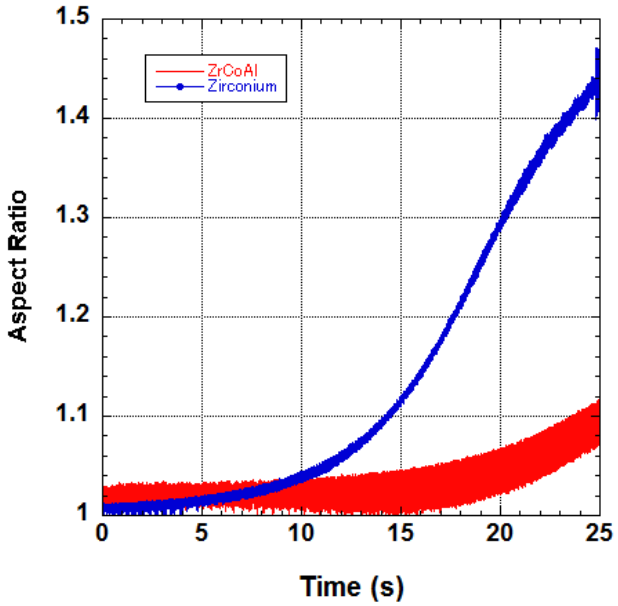


**Fig.3** Evolution of aspect ratio after bifurcation; low viscosity sample (zirconium) shows higher evolution


### Acknowledgement

This research was partially supported by a Grant-in-Aid for Science Research (B) from the Japan Society for the Promotion of Science.


### References


1) Y. Abe, S. Matsumoto, T. Watanabe, K. Nishinari, H. Kitahata, A. Kaneko, K. Hasegawa, R. Tanaka, K. Shitanishi, S. Sasaki: Int. J. Microgravity Sci. Appl. **30** (2013) 42

2) K. Ohsaka, A. Rednikov, S. S. Sadhal, E. H. Trinh: Rev. Sci. Instrum. **73** (2002) 2091

3) W. -K. Rhim, S. K. Chung, D. Barber, K. F. Man, G. Gutt, A. Rulison, R. E. Spjut: Rev. Sci. Instrum. **64** (1993) 2961

4) T. Ishikawa,P.-F. Paradis, T. Itami, S. Yoda: Meas. Sci. Technol. **16** (2005) 443.

5) W.-K. Rhim, T. Ishikawa: Rev. Sci. Instrum. **69** (1998) 3628

# 静電浮遊炉を用いた回転変形による高温融体の表面張力測定

○渡邊勇基（エイ・イー・エス），岡田純平，石川毅彦（宇宙航空研究開発機構）

# Surface Tension Measurement of Molten Melts using Deformation by Rotation using an Electrostatic Levitator

○Yuki WATANABE (AES), Junpei OKADA, Takehiko ISHIKAWA (JAXA)

## 1. Introduction

Thermophysical properties of molten material at high temperature are essential parameters for numerical simulation of casting, or other industrial manufacturing. Recently, viscous materials at molten state such as bulk metallic glass (BMG) or quasi-crystal have been investigated by many researchers. Surface tension at high temperature, one of the important properties, has been measured by oscillation method with levitation techniques. But oscillation is not applicable to viscous liquids because it is difficult to excite the sample oscillation. On the other hand, there is a rotation method to measure surface tension of viscous liquid with levitation, proposed by other researchers[1]. In this research, we apply a rotation method to electrostatic levitation. Then, we check the rotation frequency detected by laser power fluctuation reflected from sample surface with high speed video camera (HSV). Finally, we measured surface tension of ZrCoAl (BMG material) through the rotation method.

## 2. Experimental Setup and Procedures

### 2.1 Electrostatic Levitator

The measurements were made using a high vacuum ESL which can be evacuated to a ~$10^{-5}$ Pa. Detailed information about the ESL was found in elsewhere[2,3]. The levitated sample was rotated using rotating magnetic field, which was generated by four coils placed under the bottom electrode[4].

### 2.2 Surface tension measurement with rotation

The shape of levitated droplet changes with increasing of rotation speed. Surface tension is calculated from change of sample diameter with change of rotation speed. With increasing rotation speed, sample shape becomes spherical (axisymmetric with vertical axis) to like a cigar (non-axisymmetric)[5]. Therefore we can determine rotation frequency with the system shown in Fig.1.

By ESL, it is possible to levitate the sample with various viscosity, so we can observe the transition of sample shape (symmetrical - unsymmetrical) repeatedly. Theoretically, rotation frequency of sample is determined by surface tension and mass, so we can calculate the surface tension of the sample by measuring rotation frequency at shape transition precisely.

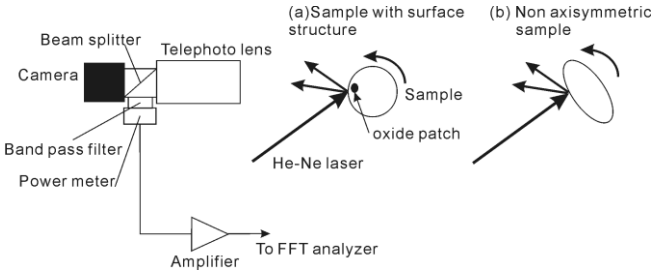


**Fig.1** Detection of rotation frequency of the levitated sample.

## 3. Results

At first, we compared with rotation frequency of Zr melt observation by HSC or detected by fluctuation of laser reflected from sample surface. These were agreed well (Fig.2).

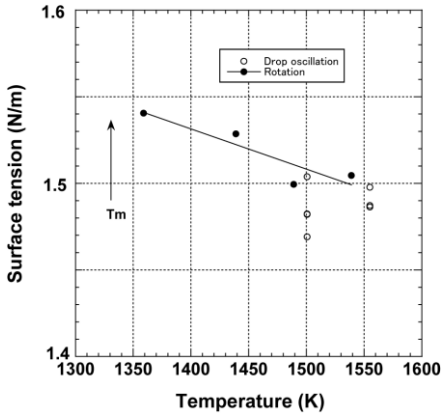


**Fig.2** Comparing rotation frequency by two method.

Experimental value by rotational / oscillation methods with molten $Zr_{55}Co_{20}Al_{25}$ sample is shown in Fig.3. Viscosity of this sample rises up near melting point ($T_m$). By rotational method, we could measure surface tension near $T_m$ which we could not apply the oscillating method.

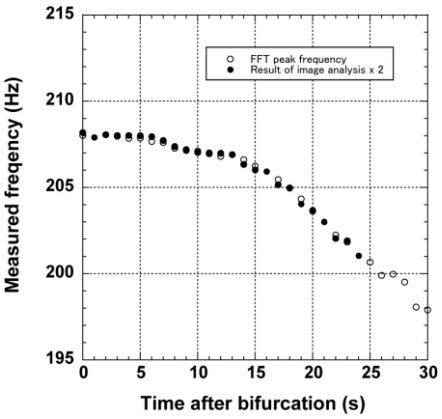


**Fig.3** Surface tension of $Zr_{55}Co_{20}Al_{25}$ sample.

## 4. Conclusion

In this paper, we tried to apply rotational method to surface tension measurement with viscous sample at high temperature. We confirmed that rotation frequency of Zr melt by HSC image analysis and FFT analysis. Also, we applied rotation method at $Zr_{55}Co_{20}Al_{25}$, surface tension could be measured at various temperature. We will study to apply rotation method for viscosity measurement.

## References


1) W. -K. Rhim and T. Ishikawa, Rev. Sci. Instrum., 72 (2001), 3572-3575.
2) Paradis P-F, Ishikawa T, Lee G W, Holland-Moritz D, Brillo J, RhimW-K, and Okada J T, Materials Science and Engineering R, 76 1-53 (2014).
3) T. Ishikawa et al. *Rev. Sci. Instrum.* **73** (2000), 2490.
4) P. -F. Paradis, T. Ishikawa, S. Yoda, *J. Jpn Soc. Microgravity Appl.* Vol.20 No.3 (2003).
5) R.A.Brown and L.E. Scriven, Proc. R. Soc. Lond. A 371 (1980), 331.

# 超高温融体のコンプトン散乱測定

○岡田純平[1,2]，P.H-L.Sit[3]，渡辺康裕[4]，石川毅彦[1]，B. Barbiellini[5]，伊藤真義[6]，
櫻井吉晴[6]，A.Bansil[5]，木村薫[4]，七尾進[4]

# Compton Scattering Experiments on High-Temperature Liquids

J. T. OKADA[1,2], P. H.-L. Sit[3], Y. WATANABE[4], B. BARBIELLINI[5], T. ISHIKAWA[1], Y. J. WANG[5], M. ITOU[6], Y. SAKURAI[6], A. BANSIL[5], R. ISHIKAWA[4], M. HAMAISHI[4], P. -F. PARADIS[1], K. KIMURA[4] and S. NANAO[1]

[1]ISAS/JAXA, [2]PRESTO/JST, [3]City University of Hong Kong, [4]The Univ. Tokyo, [5]Northeastern University, [6]JASRI/SPring-8

Levitation technique is extremely effective in studying the high temperature/undercooled liquid, since a sample vessel is not required. Recently many remarkable studies on the structural property of high temperature/undercooled liquid have been reported using the levitation technique. We applied the levitation technique coupled with Compton scattering measurements to study the electronic property of high temperature liquid.

X-ray Compton scattering is an ideal technique for probing wave functions in materials. The Compton profile $J(p_z)$ obtained from the measurement is given within the impulse approximation by

$$J(p_z) = \iint \rho(\mathbf{p})\, dp_x\, dp_y \quad , \qquad (1)$$

where $\mathbf{p} = (p_x, p_y, p_z)$ and $\rho(\mathbf{p})$ is the electron momentum density given by

$$\rho(\mathbf{p}) = \sum_j n_j \left| \int \Psi_j(\mathbf{r}) \exp(-i\mathbf{p}\cdot\mathbf{r})\, dr \right|^2 \quad , \qquad (2)$$

where $n_j$ is the electron occupation of $j$-state $\Psi_j(\mathbf{r})$. The Compton technique can also provide a novel spectroscopic window on the liquid state. Since no charged particles entering or leaving the sample are involved, the Compton technique is a genuinely bulk probe, which is not complicated by surface effects present in photoemission or electron scattering experiments.

Compton profiles of high-temperature liquids were measured by high-energy (116 keV) inelastic x-ray scattering at the BL08W beamline of SPring-8, Japan. The energy spectrum of Compton scattered X-rays was converted to the Compton profile with a momentum resolution of 0.16 a.u. The data processing to deduce the Compton profile from the raw energy spectrum consists of the following procedures: background subtraction and energy dependent corrections for the Compton scattering cross section, the absorption of incident and scattered x-rays in the sample, the efficiency of the analyzer and the detector, and correction for double scattering event. Backgrounds for the measured profiles are suppressed in the levitation technique used since no material is present in the immediate vicinity of the sample at the x-ray scattering center.

Car-Parrinello molecular dynamics (CPMD) simulations were performed with the Quantum ESPRESSO package within the framework of the density-functional theory using the generalized gradient approximation. We employed ultrasoft pseuopotentials with plane-wave expansion of the Kohn-Sham wave functions and charge density up to kinetic energy cutoff of 25 Ry and 200 Ry, respectively. The bonding character in the high temperature liquids obtained through CPMD simulation was analyzed with the maximally-localized Wannier functions (MLWFs) method where the MLWFs are obtained through an unitary transformation of Kohn-Sham wave functions. The spread is an indicator of the spatial extent of the MLWF. The MLWFs with small spreads mostly correspond to the covalent bond pairs. The MLWFs with large spreads contribute to the metallic properties. We refer to such electron pairs as diffuse pairs. The details of the experiments and analysis will be discussed in the talk.

28H04

# 「きぼう」搭載用静電浮遊炉の開発状況

○田丸晴香，大熊隼人，柚木園諭，中村裕広，石川毅彦，岡田純平（JAXA），高田哲也，新井達也，佐々木博，藤野直樹，酒井由美子（(株)IHI エアロスペース）

# Current Status of Electrostatic Levitation Furnace (ELF) for KIBO in ISS

○Haruka TAMARU, Hayato OHKUMA, Satoshi YUKIZONO, Yasuhiro NAKAMURA, Takehiko ISHIKAWA, Junpei T. OKADA(JAXA), Tetsuya TAKADA, Tatsuya ARAI, Hiroshi SASAKI, Naoki FUJINO and Yumiko SAKAI(IHI Aerospace Co. Ltd.)

## 1. Introduction

Three and a half years have passed since JAXA started the development of Electrostatic Levitation Furnace (ELF) for Kibo/ISS. We already finished the development of Engineering Model (EM), and improved the design of flight model in response to the EM test result.

The objectives of the ISS mission using ELF are to measure thermophysical properties around high melting temperature, and to quest for new functional materials by solidification including overcooling conditions. The first target sample is oxides. The melt oxides cannot be levitated by electromagnetic force and also it is difficult by Electrostatic Levitator on ground, because the electric charge of nonconductor is much less than that of conductor.

In 2012, JAXA selected one scientific experiment using ELF. Next selection of ELF utilization research will be announced by early 2015 and it is under preparation. Additionally, in August 2014, Electromagnetic levitator (EML) was launched by ATV5 and it is now assembled and is checked out for starting experiment. The containerless processing with both equipments will grow increasingly important in the future.

## 2. Current Status of Development

### 2.1 Ground function Test

With the Engineering Model of ELF, we succeeded in levitating and melting of zirconium. We also succeeded in measuring density changes, temperature changes, surface tension, and viscosity. The high-voltage amplifier and electrode interval were different from flight configuration because of gravity. We hope to get same or better data using flight model in the function test. Fig. 1 shows a density change by Overview Camera.

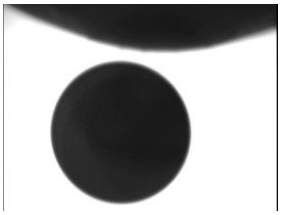

**Fig. 1** density change image

### 2.2 Unique Operation of ELF

In the usual case, ELF will be controlled through the ground system. On the other hand, some commands which must be performed quickly are transmitted and received using the laptop in ISS. Ground operators control the laptop remotely with remote desktop function via Ku two-way communication.

This way will make it easier for users to conduct experiments. For example, droplet oscillation starting, oscillation data auto-analyzing, and real-time graph displaying.

## 3. Countdown to ISS

Now we completed the flight model assembly, and then we will start various tests to confirm whether all systems work functionally. The tests include functional tesstings, off-gassing, EMC, thermal cycling, noise check, MSPR (Multi-purpose Small Payload Rack) / ELF interface check, and communication testing.

We will hold the review to confirm whether the ELF is ready to flight by early 2015. The ELF will be launched in 2015. After arriving to ISS, the ELF will be assembled by onboard astronauts, then it will be set into the MSPR in Kibo. Fig. 2 and 3 show the overview of ELF. Operations for users will be started by the end of 2015.

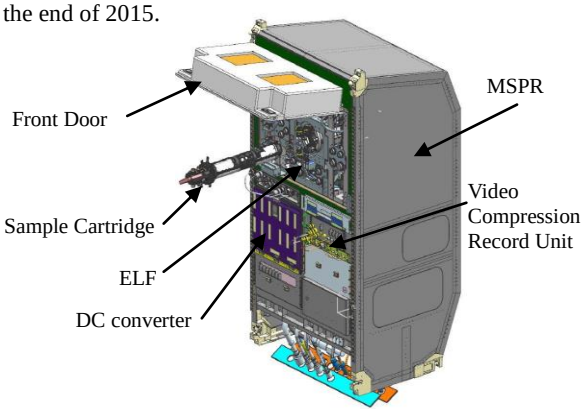


**Fig. 2** ELF in MSPR

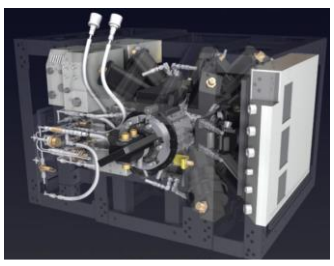

**Fig. 3** ELF Fight model image

28H05

# 鉄と酸化物メルトの界面張力測定
## －液滴振動法による界面張力測定の検討－

○渡邉匡人（学習院大），上野翔也（東北大院工），小野寺健太（学習院大），田中敏宏（阪大院工），
塚田隆夫（東北大院工），石川毅彦（JAXA），水野章敏（学習院大）

# Interfacial Tension between Steel and Oxide Melts by Surface Oscillation Analysis
## - Interfacial Tension Measurement by Modified Surface Oscillation Technique -

Masahito WATANABE (Gakushuin Univ.), Toshihoro TANAKA (Osaka Univ.),
Takao TSUKADA (Tohoku Univ.), Takehiko ISHIKAWA(JAXA), Akitoshi MIZUNO (Gakushuin Univ.)

The oscillating drop technique with surface oscillation analysis is useful for measurements of thermophysical properties of high-temperature liquid by using the levitation technique. The conventional surface oscillation analysis derives surface tension and shear viscosity of liquid even on the ground conditions. Recently, modified surface oscillation analysis of compound droplets has been tried to measure the interfacial tension of immiscible liquid system[1]. However, modified surface oscillation analysis for compound droplets combined with levitation method can be applied only in the microgravity conditions because the density difference separates two liquid parts under the ground. Therefore, we propose the measurements of interfacial tension between steel melts and molten oxides using the electrostatic levitation furnace (ELF) in ISS with modified surface oscillation analysis[2]. Interfacial tension between molten steel and molten oxides is important thermophysical properties on the industrial process control such as steel making processes and/or welding processes, therefore interfacial tension measurements without container and the substrate have been required in order to obtain temperature dependence of its without non-required elements in molten iron and molten oxides.

Our proposal method to obtain interfacial tension is based on the surface oscillation technique expanded to the compound droplets cases. The modified surface oscillation analysis method is as follows. We consider the normal mode of compound droplets consisted two incompressible fluids contacted each other with interfacial tension (Fig.1). Each fluid droplet has a normal mode frequency characterized by surface tension. For the case of compound droplet, two normal mode frequencies are derived from the eigenvalue equation same as a coupled harmonic oscillator. Two normal mode frequencies are expresses as follows;

$$\omega_{\pm}^2 = \omega_0^2 K_{\pm}\left(\frac{\tau^8}{\sigma}\frac{2}{(1+\Delta\rho)\tau^{10}+2/3\Delta\rho}\right)$$

$$K_{\pm} = \frac{1}{2}\left(\frac{\sigma m_i}{\tau^3}+\frac{m_o\tau^3}{\sigma}\right) \pm \sqrt{\frac{1}{4}\left(\frac{\sigma m_i}{\tau^3}-\frac{m_o\tau^3}{\sigma}\right)^2+1}$$

$$\tau = \sqrt{R_o/R_i},\ \ \sigma = \sqrt{\sigma_o/\sigma_{12}},\ \ \Delta\rho = (3/5)(\rho_i-\rho_o)/\rho_o$$

$$m_i = (1+\Delta\rho)\tau^5 - \Delta\rho/\tau^5,\ \ m_o = (3\tau^5)/5 + 2/(5\tau^5)$$

where, $\omega_0$ is normal mode frequency of out side fluid of surface tension of $\sigma_o$, $\sigma_{12}$ is interfacial tension, $R_{o/i}$ is radius of out side or inside fluid, $\rho_{o/i}$ is density of out side or inside fluid, respectively. From these equations, it is identified that normal mode frequency of compound droplet depends on the density difference between outside and inside fluids and the radius ratio of outside and inside fluid. Thus, we examine the change of normal mode frequency on the thickness of covered molten oxide layer by numerical simulations. Most important problem is the effect of viscosity of molten oxides. Because of, if high viscosity fluid covers on molten steel, the surface oscillation easily damps with very short time. This case we cannot measure the surface oscillation frequency. Therefore, we also examine the dependence of normal mode frequency on the viscosity by numerical simulations. On presentation, we discuss about the analysis of surface oscillation of compound droplet consisted by molten steel and molten oxides and introduce our current status of ISS experiments preparations.

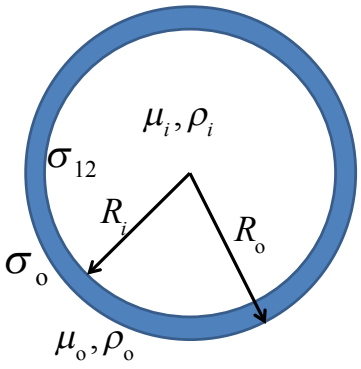


**Fig.1** System configuration of compound droplet for interfacial tension measurements.

## References

1) I. Egry *et al*., J. Mater. Sci., 45(2010) 1979.

2) M. Saffren *et al*., Proceedings of the 2nd international colloquium on drops and bubbles, (1981) 7.

3) M. Watanabe, JASMAC-27 講演予稿集，講演番号 137

# 酸素雰囲気を制御した環境下における粘性を考慮した液滴振動解析

○渡邉匡人，小野寺健太，水野章敏（学習院大），小澤俊平（千葉工大）

# Surface Oscillation Analysis of Viscous Liquid Droplets in Various Oxygen Partial Pressure Conditions

Masahito WATANABE, Kenta ONODERA, Akitoshi MIZUNO (Gakushuin Univ.) and
Shumpei OZAWA (Inst. of Chiba Tech.)

Thermophysical properties of high-temperature melts are indispensable for numerical simulations of materials processing. Accurate data are necessary to improve the process modeling, which leads to cost-effective production of high-quality products. From the requirements the levitation technique, which provides containerless conditions during the measurements, is progressed for accurate measurements of the thermophysical properties of high-temperature liquids. Therefore, we are planning thermophysical properties of high-temperature melts in the International Space Station (ISS) [1,2] using the materials-science laboratory-electromagnetic levitator (MSL-EML)[3]. Using levitation technique, thermophysical properties, surface tension, viscosity and density, are obtained from the surface oscillations of levitated liquid droplets, which is known as the oscillating drop method. Under microgravity, oscillating drop method with levitation technique has advantage of precise measurement of thermophysical properties high-temperature liquids metals. However, the liquid metals easily reacts oxygen in the atmosphere. For the reason, the surface tension shows the dependence of oxygen partial pressure ($Po_2$). $Po_2$ dependence of the surface tension using reducing gas, $H_2$, CO or $CO_2$, has been reported. For our ISS experiments using MSL-EML, these reducing gases cannot be used for the reason of hazard in ISS. Therefore, our OXYTHERM project for precise surface tension measurements of high-temperature liquids under controlled atmosphere in ISS must use the oxygen sensing and control system (OSC) based on stabilized-zirconia ($ZrO_2$) as the solid-state electrolyte. Using OSC,we can control $Po_2$ in atmospheric gas, so $Po_2$ at the sample surface can be controlled. However, since liquid metals have large solubility of oxygen at high temperature, starting samples include much amount oxygen in inside of samples. Almost initially containing oxygen diffuses out from samples, but remaining oxygen inside liquid metal samples would affect on the viscosity. Therefore, we must need to know the effect of oxygen both inside and out side of samples on the surface oscillation for using droplet-oscillating technique to measure the surface tension and viscosity. However, the effect of oxygen inside the liquid droplets on the surface oscillation has not be clarified. In order to clarify the effect of dissolved oxygen on the surface oscillation, we observed the surface oscillation of liquid Zr contained oxygen of 500 (ppm mass oxygen: PMO) and 3000PMO[3]. These samples were prepared by the ark melting of high-purity crystalline Zr samples, which is purified by the directional crystallization method, with $ZrO_2$ powders. Using electrostatic levitator, we observed the surface oscillation damping in the vacuum conditions of $10^{-4}$Pa with the function of waiting time after melting of the samples. Also, using electromagnetic levitator, we observed the surface oscillation of the same samples under the controlled $Po_2$ conditions. From the observation, we found that the surface oscillation amplitude and damping were different with the waiting time for the surface oscillation generated after melting of the samples. The damping time difference is caused by the out-diffusion of oxygen in liquid Zr from inside to the atmosphere. If oxygen completely diffuses out from inside of droplets, we will be able to obtain the viscosity value of pure liquid Zr. However, if oxygen still remains inside droplets, the viscosity shows large value rather than that of pure liquid Zr. In the case of large viscosity values, the surface oscillation frequency showed also different values from the samples without oxygen addition. This is attributed by the surface segregation of oxygen at the surface areas. The surface oscillation frequency changes with atmospheric oxygen partial pressure $Po_2$[4]. Therefore, we must care of the surface oscillation frequency analysis in different $Po_2$ conditions including the effect of out-diffusion of dissolved oxygen into the samples. We are planning to clarify the effect of out-diffusion of dissolved oxygen on the surface oscillation frequency under long time microgravity conditions using MSL-EML of ESA facility in ISS with oxygen dissolved Zr samples.

This work was supported by JAXA-WG and also by JSPS KAKENHI Grant Number 24360316.

**References**

1) H.-J. Fecht *et al*., Europhysicsnews, 39 (2008)19.

2) I. Egry and D. Voss, J. Jpn. Soc. Microgravity Appl., 27 (2010) 178.

3) T. Harada et al., MRS Online Proceedings, Vol. 1528(2013) Paper No.426.

4) S. Ozawa et al., J. Appl. Phys., 107 (2010) 014910.

28A01

# 微小重力場での過電流による難燃被覆導線の着火

○小松賢史，藤田修（北海道大学）

# Ignition of Overloaded Electric wire Insulated by Fire Retardant Material in Microgravity

○Yoshifumi KOMATSU, Osamu FUJITA (Hokkaido Univ.)

## 1. Introduction

One of the causes of fire in spacecraft is ignition of electric wire. The wire ignition is generally started with short circuit or overloading. Therefore, it is important to know the ignition characteristics of electric wire by overloading in microgravity.

In the previous research[1, 2], we clarify that ignition limit of electric wire is extended in microgravity than normal gravity. We also clarified the influence on ignition limit and ignition delay time by oxygen concentration, pressure, and so on. In the studies we used single PE-NiCr wire to investigate the phenomenon. However, single PE wire is not practical one because PE has high flammability and practical shape in actual use is not single wire but two or more twisted wires.

In this study, therefore, we investigate the difference of change in ignition limit by gravitational condition (1G and micro G) between PE wire and ETFE (fire retardant material) wire in the shape of twisted wire.

## 2. Experimental method

Fig.1 shows the outline of experimental chamber. It is composed of a combustion chamber with sample wire, DV camera, and Current source.

Two types of wire shape, single and twisted wire as shown in Fig.2, are compared in terms of ignition limit with PE insulation wire and, then, flammability of PE and ETFE insulated wires in twisted shape are compared to know their flammability difference.

To obtain microgravity environment, we use the HASTIC drop tower (“COSMOTORRE”, Akabira, Hokkaido, μG: 2.5s).

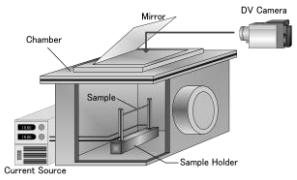


**Fig.1** Outline of experimental chamber

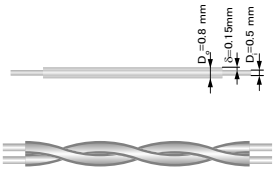


**Fig.2** Outline of sample wire

## 3. Result and discussion

First, we consider the effect of wire shape. Fig.3 shows the ignition limit of single wire and twisted wire at 1G by using PE. From Fig.3, it seems that the twisted shape has an effect to extend the ignition limit.

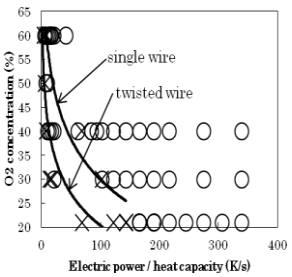


**Fig.3** Comparison the ignition limit between single and twisted wire at 1G (PE)

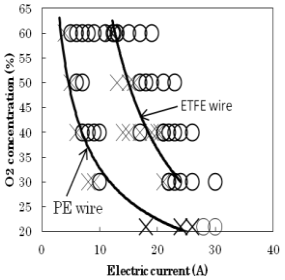


**Fig.4** Comparison the ignition limit between PE and ETFE wire at 1G (twisted wire)

**Table 1** Ignition delay time at each situation (twisted wire)

| Insulation material (1G or μG) | O2 concentration (%) | Current value(A) | Ignition delay time (s) |
|---|---|---|---|
| PE (1G) | 40 | 17 | 2.40 |
| PE (μG) | 40 | 17 (ignition limit) | 2.23 |
| ETFE (1G) | 40 | 21(ignition limit) | 2.17 |
| ETFE (μG) | 40 | 21 (ignition limit) | 2.17 |

Second, we investigate the effect of materials. Fig.4 shows the ignition limit of PE and ETFE wire at 1G (twisted wire). From the results, the ignition limit of PE wire is wider than of ETFE wire. Table 1 shows the comparison between 1G and μG. According to the table, difference by the difference of gravity condition is unclear for both of PE and ETFE. This is because (1) μG time is too short to discuss the difference of ignition limit, and (2) twisted of wire may lead to smaller difference of ignition limit. Therefore, we need to make more research about the difference using longer microgravity time.

## 4. Conclusion

1. The shape of twist has an effect to extend the ignition limit.
2. The effect of microgravity is small with twisted ETFE wire, which may be caused by the reduced microgravity effect in twisted shape.

## Acknowledgement

The authors appreciate JAXA for their support in conducting the research on “Solid Combustion” and “FLARE”.

## References

1) H. Noda et al., JSME, MECHJ-5, vol 5, pp459-460, (2005)

2) K. Agata et al., International Journal of Microgravity Science and Application, vol25, No.1, pp11-16, (2008)

28A02

# 微小重力下で対向流を受ける薄い平板試料の可燃限界

○高橋周平，坪井寛大，井原禎貴（岐阜大）

# Flammability Limit of a Thin Flat Material with an Opposed Flow in Microgravity

○Shuhei TAKAHASHI, Kandai TSUBOI, Tadayoshi IHARA (Gifu Univ.)

## 1. Introduction

The flammability test for materials used in space environment has been checked by the so called NASA STD-6001, which is a pass/fail test conducted in normal gravity [1]. On the other hand, it has been reported that the flammability limit or limiting oxygen concentration in microgravity environment may expand in a certain condition [2, 3]. Many materials has been tested it flammability on ground, like as LOI method (JIS K7201) and the accumulated database are valuable. Therefore, it is very important to clarify the difference between the flammability limits in normal gravity and microgravity.

In the Solid Combustion and FLARE projects [4], ISS Kibo module experiments, supported by JAXA, we are discussing new criteria of fire safety for solid materials used in space environment. For flat materials, we first have obtained the flammability map of a PMMA sheet with an opposed flow to propose an extinction model in various conditions. In this article, we show the obtained flammability map by parabolic experiments and compare the extinction limit with the prediction by the model.

## 2. Experimental Setup and Scale Modeling

### 2.1 Experimental Apparatus for Parabolic Flight

The flammability limit of a thermally thin PMMA sheet (Acryplen: Mitsubishi Rayon Co., Ltd.) was investigated in microgravity. The thickness of the sample was 125μm. The width and the length are 2cm and 12cm, respectively. The sample was put between metal guide plates and set in a small wind tunnel with a suction fan, rectifying honeycomb meshes, and a Ni-Cr igniter (see Fig. 1). The microgravity environment was attained by parabolic flight by DAS for 20s. The sample was ignited at the onset of microgravity environment, and the flame spread rate and the surface temperature are measured by a visible CCD camera and an infrared camera. The opposed flow velocity and the oxygen concentration were varied as parameters.

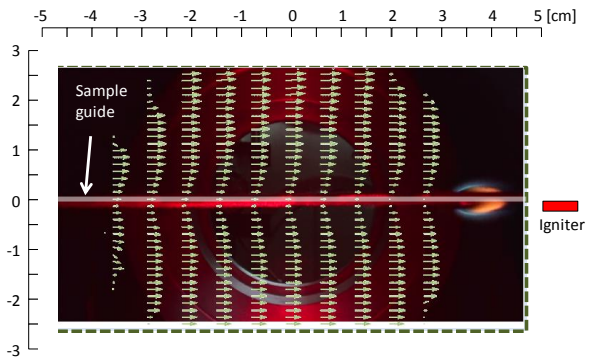


**Fig. 1** Test section of the experimental apparatus.

### 2.2 Scale Analysis

We built up scale modeling of heat transfer in the flame spread over a thermally thin material [5]. Figure 2 shows the schematic of the flame used. Since the radiation loss and the kinetic effect were considered as the suppression factors of flame spread, the heat balance equation is expressed as follows,

$$V_f \rho_s c_s \tau W (T_v - T_\infty) + \varepsilon (1 - a_{abs}) \sigma (T_v^4 - T_\infty^4) L_{sx} W \sim \left(1 - \frac{1}{Da}\right) \cdot \lambda_g \frac{(T_f - T_v)}{L_{gy}} L_{gx} W \quad (1)$$

In this equation, the second term of left hand side and the factor appears in the right hand side are the radiation loss and the kinetic effect, respectively. Non-dimensionalizing Eq. (1) by the flame spread rate in thermal regime [6], we obtained a simple equation,

$$\eta + 1/Da_R + 1/Da = 1 \quad (2)$$

$$Da_R \sim \frac{\rho_g c_g V_r (T_f - T_v)}{\varepsilon (1 - a_{abs}) \sigma (T_v^4 - T_\infty^4)} \quad (3)$$

$$Da \sim \frac{\alpha_g}{V_r^2} \rho_g Y_O A \exp(-E / RT_f) \quad (4)$$

where $Da_R$ is the radiation (fourth) Damköhler number [5] and $Da$ is the first Damköhler number, respectively. In Eq. (2), we assumed that the extinction occurs at $\eta$~0.

## 3. Results and Discussion

The obtained flammability map is shown in Fig. 2. The number beside the symbol means the spread rate in mm/s. The limiting Oxygen Index (LOI) was found to be 17.0% by the ground downward spread tests. In microgravity environment,

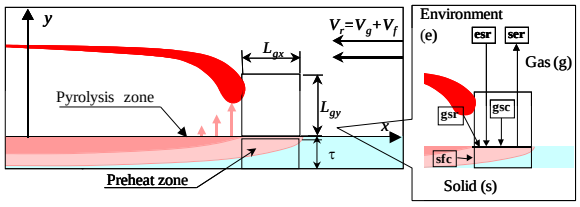


**Fig. 2** Flame spread over a thin material.

the flame spread was possible even below the LOI. The minimum limiting oxygen concentration (MLOC) was 14.7%, which was 2.3% lower than the LOI. The opposed flow velocity near the MLOC condition was observed was about 6~10cm/s. The predicted flammability limit by Eq. (2) is also shown in Fig. 2. The model underestimated the MLOC about 1.7%, but reproduced the profile of the limiting line properly. The predicted opposed flow velocity at the MLOC condition was 8cm/s, which agreed with the experimental result.

We also conducted the flammability test changing the diluent gas from nitrogen to carbon dioxide as well. Carbon dioxide has large specific heat and small temperature diffusivity; therefore, it was predicted that the flame spread was possible at very low opposed flow and the difference between the LOI and the MLOC became large. Figure 3 shows the flammability map and the predicted limiting line. It is found that flame spread was possible when the opposed flow velocity was very low, 2cm/s, whereas extinction occurred at the same opposed flow velocity in nitrogen balance condition. The LOI was 24.3%, and the MLOC was 19.2%. It is found that the margin between the LOI and the MLOC was 5.1%, which was larger than that in nitrogen balance condition. Thus, the trend in carbon dioxide balance condition was captured by the model. Although the developed model underestimated the MLOC, it could predict the effect of ambient gas properties correctly. Bhattacherjee et al. reported that the non-dimensional spread rate η become 0.5 at extinction condition [7]. Hence, the assumption $\eta$~0 may be too strong. For more accurate prediction, the extinction assumption should be modified.

## 4. Summary

The flammability limit of thin PMMA sheet was obtained and the effect of the diluents gas was clarified. The developed model could capture the trend of extinction near MLOC and the effect of ambient gas properties, but it still under estimate the MLOC. The modification of the extinction assumption may be needed.


## Acknowledgment

This study was supported by JAXA and JSF as Solid Combustion and FLARE projects.


## References


1) NASA-STD-6001 B: Flammability, Offgassing, and Compatibility Requirements and Test Procedures (2011).

2) O. Fujita, M. Kikuchi, K. Ito, S. L. Olson, T. Kashiwagi and T. Sakurai: J. Jpn. Soc. Microgravity Appl., 14, 1(1997) 25 (in Japanese).

3) A. Kumar, H. Y. Shih and J. S. T'ien, Combustion and Flame 132 (2003) 667.

4) O. Fujita, J. Combustion Society Japan 56, 176 (2014) 117 (in Japanese).

5) S. Takahashi, M. Kondou, K. Wakai, S. Bhattacharjee, Proc. Combustion Institute, 29 (2002) 2579.

6) S. Bhattachrjee, J. West, and R. A. Altenkirch, Proc. Combust. Inst. 26 (1996) 1477.

7) S. Bhattacharjee, K. Wakai, S. Takahashi, Combust. and Flame, 132 (2003) 523.


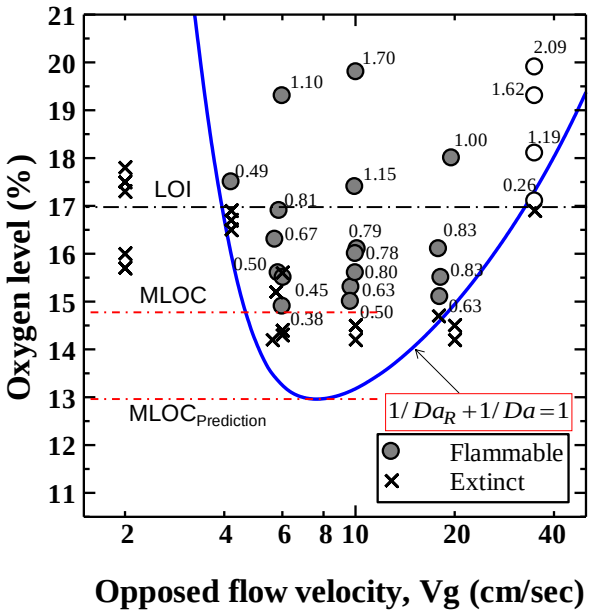


**Fig. 3** Flammability map and the predicted extinction limit for nitrogen balance condition.

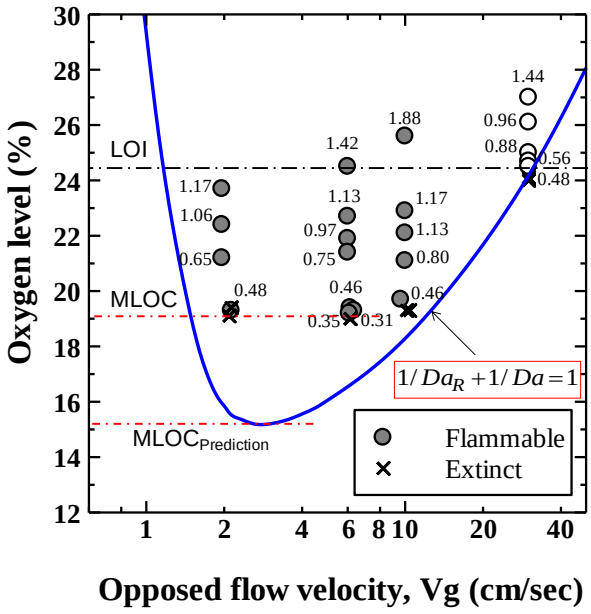


**Fig. 4** Flammability map and the predicted extinction limit for carbon dioxide balance condition.

28A03

# LOI に与える重力影響に関する考察

○中村祐二（豊橋技科大），細貝亜樹（JAXA），若月　薫（消防研究センター）

# A Study of Potential Gravity Effect on LOI

○Yuji NAKAMURA (Toyohashi Univ. Tech.), Aki HOSOGAI (JAXA), Kaoru WAKATSUKI (NRIFD)

## 1. Introduction

### 1.1 Do We Have a Problem in Selection of Fire Safeness Material in Space?

To ensure the fire safeness in space, the material to bring into ISS (International Space Station) must be passed the qualification test. Currently NASA-STD-6001[1] is the major protocol for this purpose based on the pass/fail criteria for upward flame propagation process. Since the upward flame propagation is believed to *always* give the most hazardous fire scenario, this test is widely recognized as "conservative" one (namely it should adopt the fire in any gravity environment). Because NASA-STD-6001 was originally designed to the specific environment as ISS, NASA recently proposed the extended methodology based on "ULOI (Upward Limiting Oxygen Index)" to adopt various type of space habitants. This is the test to check whether the material could continuously burns under which oxygen concentration in upward propagation system. Again, upward propagation is the most conservative test, oxygen concentration below ULOI should be safe in fire. However, what happens if the "conservative" assumption is not valid (in other word, say, minimum oxygen concentration becomes much lower when the exposed gravity is reduced)? Unfortunately, at very near the extinction limit, it is suspected that the judgment with upward propagation system under normal gravity does really give the most "dependable (i.e., conservative)" limit.

Consider that oxygen concentration decreases gradually to find the extinction point under normal gravity. One expects that the flame becomes very weak and be so sensitive to the ambient flow. Eventually, flame shall be experienced the blow-off because of the relatively strong buoyancy-induced flow. In this sense, the limit must be given always as blow-off criterion. On the contrary, as the buoyancy-induced flow decreases (i.e., most likely the imposed gravity is reduced), the flame could potentially stay there since there is little flow disturbance. Instead, under such condition, diffusive transport starts to play a role and extinction will be somehow triggered by conductive (or radiative) loss in the system. In other word, conductive/radiative heat balance will determine the limit under low gravity. Considering altogether, to know the "conservative" limit under microgravity environment, conductive/radiative heat balance in either concurrent/opposed flow system must be properly modeled and examined.

### 1.2 Objective in this Study

Research target is now clear and all we need to study is how much we could find the "largest" difference between the limit under normal gravity and the one obtained under low gravity environment. To examine this issue, we must select the most appropriate experimental design, namely, what kind of test condition could give the most sensitive to the gravity. This is objective and motivation in this study.

Meanwhile, in this work, we only consider about the very low gravity since the limit under normal gravity in upward flame propagation system could be obtained by elsewhere (e.g., NASA). Because the target condition is the very low gravity, at which diffusive transport is dominant, flowing direction against the spreading direction of the flame does not matter. Thus the test is performed with opposed-flow system and the quantity to be compared is LOI (Limiting Oxygen Index).

## 2. Experiment

In this study, LOI is obtained by the protocol described in ISO4589-2[2]. Facility, procedure of the test and typical flame obtained are shown in Fig.1.

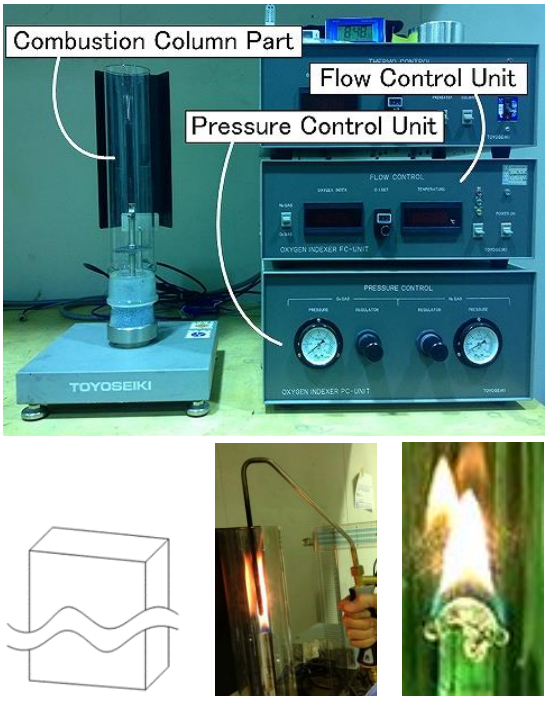


**Fig.1** LOI test facility: (top) test system, (bottom left) specimen, (bottom center) ignition procedure, (bottom right) typical flame spreading toward the downward.

According to the ISO protocol, the top surface of the specimen (10mm width and 4mm thickness) is heated by the propane burner flame to achieve flaming. The candle-like flame is established over the specimen and moves down as the material is consumed. During the burning event, specimen tends to melt (if it is the melting material) and the molten layer is formed surrounded the top surface.

## 3. Results and discussion

### 3.1 Limiting Flame Configuration for 4mm-thickness Sample

Fig. 2 shows the representative of the limiting flame formed over the standard PMMA specimen followed by ISO protocol (namely, the thickness of the specimen is 4 mm).

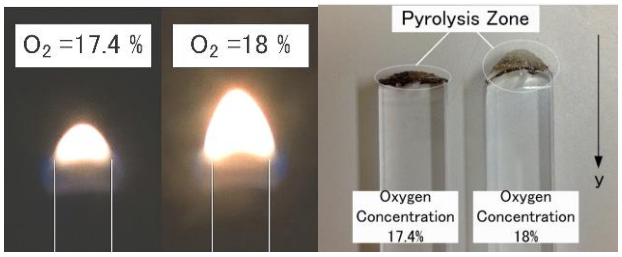


**Fig.2** Candle-burning test of PMMA (whose LOI is 17.34) under different oxygen atmosphere (17.4% and 18%). Flame at 17.4% O2 is the very near the extinction condition (sufficient to call "limiting flame")[3)]

As indicated in the figure, flame becomes shorter when the limiting condition is approached. Moreover, as found in the right pics, edge of the flame is close to flat. It is understood that the small flame is attached over the surface and the fuel regression is continuously done along the specimen. The latter feature reminds us that the combustion system would show "less-dimension" feature and it is approached to most likely 1-D flame system.

### 3.2 Limiting Flame Configuration for 1mm-thickness Sample

Fig. 3 shows the another representative of the limiting flame formed over the "thinner" PMMA specimen whose thickness is 1 mm (quarter of the standard one).

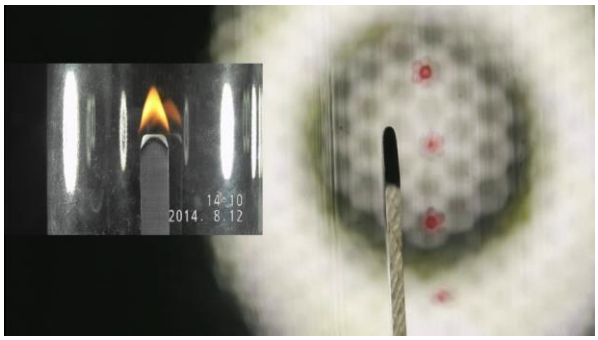


**Fig.3** Flame at 0.2%-higher-than-extinction-O2 formed over 1mm thickness PMMA sample. Front image is enbedded in the figure with backrigh image (side view)

It is rather obvious that the flame is elongated toward the upstream (which is bottom direction in the figure) and the regression of the specimen is not likely 1-D as suggested by Fig.2. Moreover it seems that two side flame covers the specimen side-by-side. In this sense, this flame system remains the dimensional feature (not likely 1-D).

### 3.3 Effect of Thickness on Limiting Flame and Their Dependency on Gravity

Let us consider the very thick limit and very thin limit of the sample and what kind of flame system would be appropriate to assume. It is understood that the thicker sample tends to less-dimension and thinner sample does not (rather 2-D like flames appears). Thus the applicable flame system would be summarized as following figures (Fig3)

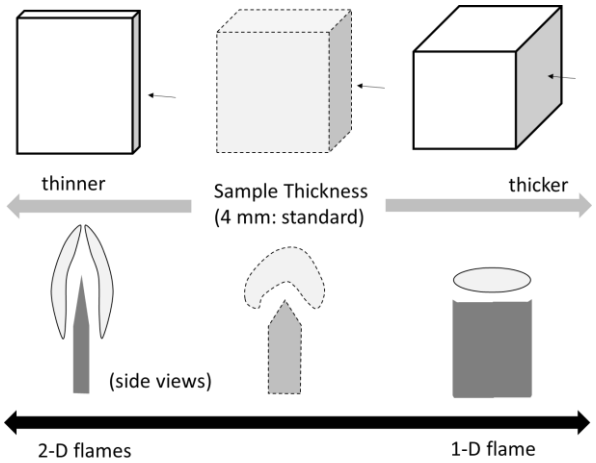


**Fig.3** Applicable flame model depending on the sample thickness

If this consideration is valid, gravity effect must be more pronounced in thinner sample so that effect of the gravity must appear to such specimen. In other word, it is less-pronounced the gravity effect on standard sample described by ISO protocol to measure LOI. We will continuously work on this issue in future under the monitoring the FLARE project.

## Acknowledgments

This work is conducted as part of the study of prioritized research proposals of JEM utilization (FLARE project).

## References

1) NASA-STD-6001;Flammability, Odor, Offgassing, and Compatibiliyy Requirements and Test procedures for Materials in Environments that Support Combustion, NASA (Feb. 9, 1998)
2) ISO4589-2 Plastics-Determination of burning behaviour by oxygen index Part 2: Ambient-temperature test
3) K. Kizawa: Bachelor Thesis approved by Hokkaido University (supervisor: Y. Nakamura), 2014.3.

# ISS「きぼう」における固体材料燃焼実験(Solid Combustion)　第二報

○水島隆成，菊池政雄，高柳昌弘（JAXA），鳥飼宏之，伊藤昭彦（弘前大），
高橋周平（岐阜大），藤田修（北大）

# Overview of "Solid Combustion" Experiment in the ISS/KIBO

○Takanari MIZUSHIMA, Masao KIKUCHI , Masahiro TAKAYANAGI (JAXA), Hiroyuki TORIKAI, Akihiko ITO (Hirosaki Univ.), Syuuhei TAKAHASHI (Gifu Univ.), Osamu FUJITA (Hokkaidou Univ.)

## 1. Introduction

A lot of astronauts have been staying in the International Space Station(ISS) for long term. They have carried out many scientific experiments in the microgravity environment. To secure their safety, the protection against fire is a particularly important issue. However, the current material flammability tests for fire safety in space are performed in the normal gravity, and it is known that the material flammability could be enlarged in microgravity in some conditions[1]-[4] .Therefore it is necessary to understand the impact of gravity on the the material flammability.

In JASMAC-26, we introduced the main objectives of Solid Combustion. In this report, we will introduce the contents of each experiment.

## 2. Overview of the Experiment

### 2.1 Objectives

Our research entitled “Quantitative Description of Gravity Impact on Solid Material Flammability as a base of Fire Safety in Space(Solid Combustion)“ will be carried out in the Japanese Experiment Module/KIBO in the ISS. The main target of the research is to clarify the impact of gravity on the the material flammability.

In this research, we will carry out four kinds of experiment to obtain the ignition map of overloaded wire and flammability map of spreading flame.

Table 1 shows the sample and the expected data map in each experiment.

### 2.2 Experiment 1

We define the marginal condition in which the wire covering is ignited. Then we clarify the mechanism which define the marginal condition for the case that an over-current flows into the polyethylene insulated wire.

Fig.1 shows the experimental apparatus. It has the reals and motors to wind the wire. The wire is electrified with the electric pole. Then we will investigate the presence or absence of ignition.

### 2.3 Experiment 2

We define the marginal condition that the flame spreading on the wire covering maintain the oneself. Then we clarify the mechanism which the marginal condition is determined.

The experimental apparatus is similar as the experiment 1. Although, the ignition wire is utilized instead of electric pole. Forced ignition is carried out to the wire. After that, the apparatus controls the speed to maintain the flame and melting sphere in one position. Then we will observe the flame and sphere with the camera such as high-speed camera and IR camera.

### 2.4 Experiment 3

We quantify the spreading speed and the preheated sizes of the PMMA sheets. Then we clarify the extinction limit conditions and review the prediction obtained from scale analysis.

Fig.2 shows the concept of the experiment. With two metal frames, PMMA sheet and ignition wire are sandwiched.

With the ignition wire, forced ignition is carried out. Then we observe the flame which is spreading on the sheet.

### 2.5 Experiment 4

Experimental content is same as experiment 3. We utilize the filter paper which is the charring sample instead of PMMA sheet.

In this experiment, we clarify the effect of the existence of the char and the deference of the width on flammability limit.

**Table 1** Experiment in Solid Combustion

| | **solid material** | **expected data map** |
|---|---|---|
| Experiment 1 | polyethylene insulated wire | **ignition map of overloaded wire** |
| Experiment 2 | polyethylene insulated wire | **flammability map of spreading flame** |
| Experiment 3 | plastic sheet | |
| Experiment 4 | filter paper | |

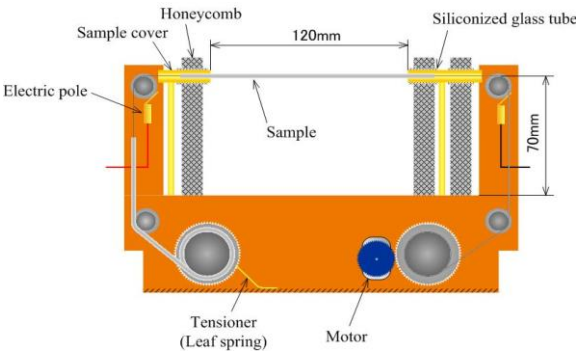


**Fig. 1** Experimental apparatus for experiment 1

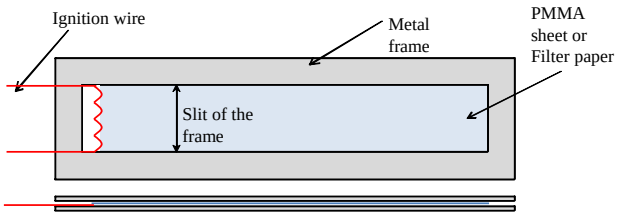


**Fig. 2** Concept of experiment 3 and 4

## References


1) K.agata, et al., *J.Jpn.Soc.Microgravity Appl.*, **VOL.25 No.1**, pp.11-16,2008.1.
2) O.Fujita, *J.Jpn.Soc.Microgravity Appl*., **VOL.28 No.3**, pp.90-95,2011.
3) Y. Onishi, et al., Transactions of the Japan Society for Aeronautical and Space Sciences, **Vol.8**, pp.Ph_19-Ph_24, 2010.
4) O.Fujita, et al., *Proc.Combustion Institute*, **VOL.33, Issue2**, pp.2617-2623,2011.

28A05

# 微小重力環境を利用した微燃性冷媒の燃焼性評価

○滝澤賢二，徳橋和明，近藤重雄（産総研）

# Flammability Evaluation of Mildly Flammable Refrigerants using Microgravity Environment

○Kenji TAKIZAWA, Kazuaki TOKUHASHI, Shigeo KONDO (AIST)

## 1. Introduction

In recent years, development of new alternative refrigerants having low global warming potentials (GWP) have been addressed. In general, to shorten atmospheric lifetime, which results in reduction of GWP, leads to an increase in reactivity with air, and consequently increases flammability. To develop environmentally friendly materials, we should consider such tradeoff relationships, that is, to minimize environmental impact without compromising fire safety for practical use. Accordingly, the demand for evaluating flammability of mildly flammable compounds has been increased.

We have reported on burning velocity ($S_u$) measurement of fluorinated compounds using the closed vessel methods [1]. As the first method we directly measured the flame radius ($r_f$)-time development in the prepressure period of combustion by the schlieren photography (SP) technique. As the second one, we used the spherical-vessel (SV) method, in which we measured pressure-time development and obtained $S_u$ by employing a spherical flame propagation model. The model was originally established for small hydrocarbons [2,3] and we applied the model to hydrofluorocarbons. However, for mildly flammable compounds with $S_u$ below 5 cm $s^{-1}$, the flame propagated so slowly that it moved upwards and was distorted by buoyancy, as shown in **Fig. 1(a)**. Since the flame propagation was different from the spherically propagating flame of highly flammable compounds, it is necessary to check the validity of the obtained data. We added experiments in $\mu$g environment, where the buoyancy does not work and $S_u$ from the spherically propagating flame will be obtained.

## 2. Experiments using a 10-m drop tower

The $\mu$g experiments were performed using a 10-m drop tower in AIST Hokkaido center. We carried out the $\mu$g experiment using the same vessel, ignition system, and recording system as the 1G experiment. Accordingly, all the differences in the results will come from the effects of gravity. To reduce the effects of ignition spark and curvature (stretch) on the flame, relatively large vessel was used (inner diameter of 155 or 200 mm). Because the SP method system was difficult to be set in the current falling capsule, the flame images were recorded directly with a high-speed video camera.

## 3. Results

**Fig. 1(b)** shows flame propagation of R-1234yf ($CH_2$=$CFCF_3$)/air in $\mu$g. Different from the data in 1G, the data in $\mu$g will abstract the intrinsic flammability characteristics that is not perturbed by the effect of the gravity. **Fig. 2** shows $S_u$ for R-32 ($CH_2F_2$) and R-1234yf together with literature data. According to Saburi and Wada [4], flame front of R-32 kept smooth during propagation in 1000 mm diameter vessel for equivalence ratio ($\phi$) in the range 0.9-1.2. Wrinkling due to hydrodynamic instability was not observed for mildly flammable compounds. We also obtained quenching distance of mildly flammable compounds. Using these data, we obtained a good relationship between $S_u$ and quenching distance for highly to only mildly flammable compounds, which will be presented in the conference.

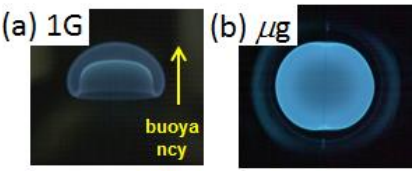


**Fig. 1** Direct flame image of R-1234yf at $\phi$ =1.32 in (a) 1G and (b) $\mu$g. $S_u$ is ca. 1.5 cm $s^{-1}$

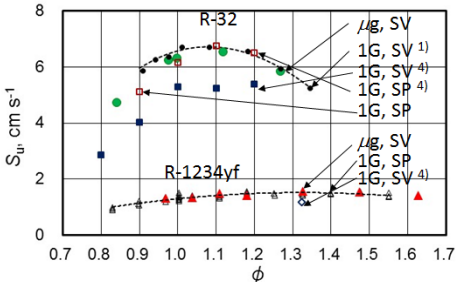


**Fig. 2** *S*u of R-32 and R-1234yf as a function of $\phi$.

## 4. Future work

We are planning to set up a 15-m drop tower in AIST Tsukuba center. We will utilize the facilities not only for further development of evaluation of low flammable materials but also for collaboration with institutes and companies.

## References

1) K. Takizawa, A. Takahashi, K. Tokuhashi, S. Kondo and A. Sekiya, Combust. Flame, **141** (2005) 298.

2) M. Metghalchi and J. C. Keck, Combust. Flame, **38** (1980) 143.

3) P. G. Hill and J. Hung, Combust. Sci. Technol., **60** (1988) 7.

4) T. Saburi and Y. Wada, JSRAE 2013 Progress Report (in Japanese) (2014) 68.

28A06

# 列方向移動可能液滴間を燃え広がる火炎が液滴の運動に及ぼす影響

○菅沼祐介，野村浩司（日本大学），三上真人（山口大学），菊池政雄（JAXA）

# Motion of Movable Droplets Induced by a Flame Spreading between Movable Droplets

○Yusuke SUGANUMA, Hiroshi NOMURA (Nihon Univ.), Masato MIKAMI (Yamaguchi Univ.),
Masao KIKUCHI (JAXA)

## 1. Introduction

Spray combustion is widely employed for industrial combustors such as diesel, jet engines, and industrial furnaces. Because spray combustion is a complicated phenomenon, there are still unknown areas in the spray combustion mechanism. Therefore various approaches have been applied to investigate spray combustion. In most of investigations focusing on fuel droplet array combustion, the droplet array consists of fixed droplet. During real spray combustion, fuel droplets move freely, relative to other droplets. Droplet motion caused by flame spreading, and the influence of the droplet motion on flame spreading, are also important areas for research. In the present work, a fuel droplet array with plural movable droplets is employed to investigate flame spreading between movable droplets. Microgravity experiments will be conducted with the group combustion experiment module (GCEM) installed into the multi-purpose small payload rack (MSPR) on the international space station (ISS). *n*-decane is employed as a low-volatile fuel, in contrast to the FLEX-2J NASA experiments [1] in which n-heptane is examined as a high-volatile fuel. In this report, the ground-based experimental apparatus and the results obtained under normal gravity conditions were presented.

## 2. Experimental Apparatus and Procedure

Figure 1 illustrates the employed experimental model of a linear fuel droplet array. Four fixed droplets and two movable droplets were dispensed along a horizontal thin fiber. The droplet closest to the igniter was referred to as the first fixed-droplet. The four fixed droplets were employed in order to suppress the influence of disturbance due to the ignition process of the first fixed-droplet on the motion of movable droplets. Movable droplets were suspended directly on the thin fiber to be allowed to move freely in the direction of the thin fiber.

The ground-based experimental apparatus consists of the droplet-array suspension system, a droplet-array slider, a droplet generator, an igniter, a high speed camera, and a sequencer as shown in Fig. 2. Behavior of movable droplets and a spreading flame were observed with the high-speed video camera. The horizontally-fixed fiber of 78 μm in diameter and 30 mm in length allows us to suspend droplets of 0.8 mm in diameter. Movable droplets were very weakly anchored at predetermined locations. One anchor point consists of two

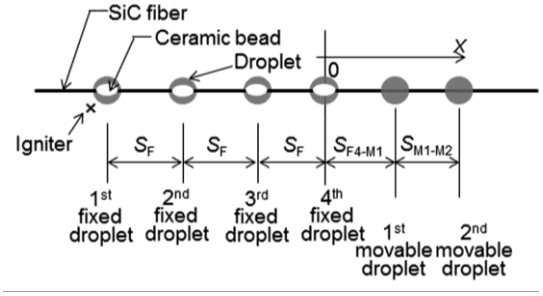


**Fig. 1** Experimental model.

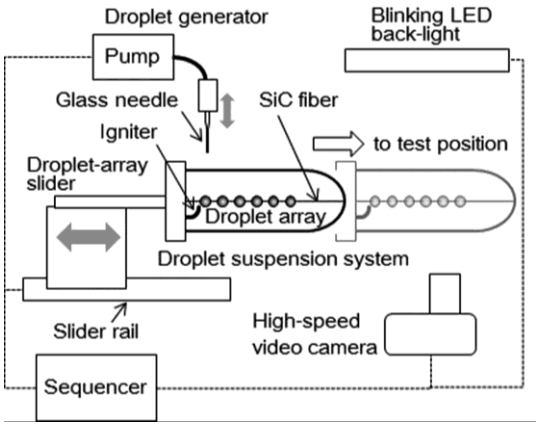


**Fig. 2** Ground-based experimental apparatus.

slightly-thinner zones etched by a $CO_2$ laser. Experiments were performed at atmospheric pressure, room temperature, and normal gravity. As a liquid fuel, n-decane was employed. Each center-to-center distance of the fixed droplets was set at 1.6 mm ± 10% for all tests.

The initial spacing between the fourth fixed-droplet and the first movable droplet and the initial spacing between the two movable droplets were varied. Initial diameter of all droplets used for the calculation of averaged initial diameter was regulated within the range of 0.8 mm ± 5%.

## 3. Experimental Results and Discussion

Flame-spread between the first and the second movable droplets was observed with varying the initial spacing between the movable droplets. The initial spacing between the fourth fixed-droplet and the first movable droplet was set at 1.38 mm or 1.42 mm (1.40-1.44 mm), which are below the initial droplet

spacing of the flame-spread-limit from a fixed droplet to a movable droplet. It was found that behaviors of spreading flame were classified into four patterns. Figure 3 shows four typical histories of the positions of the first and second movable droplets. Flame spread pattern changes from the pattern 1 to 4 as the increase in the initial spacing between two movable droplets.

Pattern 1 (Fig. 3a): This pattern was observed when the initial spacing between two movable droplets was narrow. When a spreading flame reached the fourth fixed-droplet, the first movable droplet started to move in the positive direction. At 0.058 s, the flame spread to the first movable droplet. The first movable droplet in the group-flame continued to move in the positive direction and collided against the second movable droplet. The flame around the first movable droplet was extinguished by the collision. It is supposed that the sudden temperature drop due to the coalescence with the cold second droplet led to the flame extinction of the first movable droplet. After the flame extinction, the coalesced droplet continued to move in the positive direction.

Pattern 2 (Fig. 3b): Flame extinction did not occur after the coalescence of the first and second movable droplets. The duration between the ignition of the first droplet and the coalescence was longer than in the case of the pattern 1. After the collision, the coalesced droplet continued combustion and stopped moving.

Pattern 3 (Fig. 3c): Flame spread from the first movable droplet to the second movable droplet without collision. After the flame-spread, the both movable droplets continued combustion and stopped moving.

Pattern 4 (Fig. 3d): Flame did not spread from the first movable droplet to the second movable droplet and the second movable droplet escaped from the burning first movable droplet. The first movable droplet stopped moving after the second movable droplet started moving. The second movable droplet kept moving after the first movable droplet stopped moving.

At narrow initial spacing between the fourth Fixed-droplet and the first movable droplet, another flame spread pattern was observed, which was shown in Fig. 4. The behavior of the new flame spread pattern was the same as the pattern 2 until collision of the first and second movable droplets occurred. However, the coalesced droplet accelerated towards the fixed droplets. In the case of the pattern 2, the flame of coalesced droplet was isolated. On the other hand, in this case, the coalesced droplet was surrounded by the group combustion flame together with the fixed droplets. This fact means that the coalesced droplet was heated by the group combustion flame mainly from the other side of the fixed droplet. It was supposed that asymmetric evaporation of the coalesced droplet generated the thrust towards the fixed droplet.

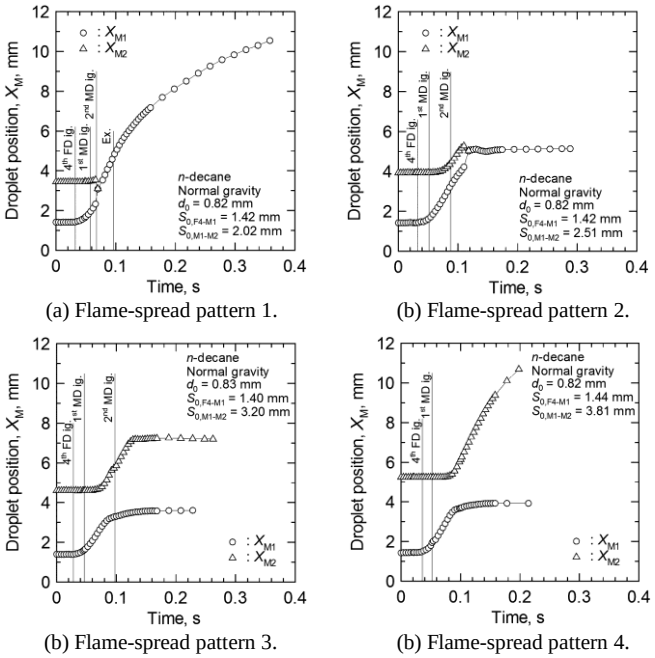


(a) Flame-spread pattern 1. (b) Flame-spread pattern 2.

(b) Flame-spread pattern 3. (b) Flame-spread pattern 4.

**Fig. 3** Histories of movable-droplet position [1].

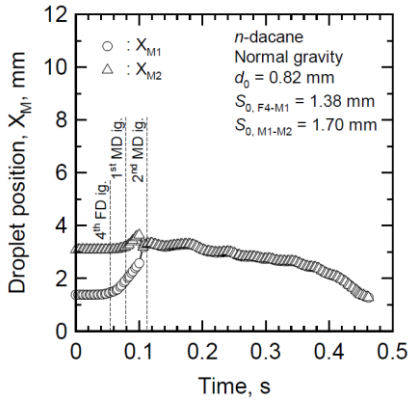


**Fig. 4** Histories of movable-droplet position at movable droplet spacing of 1.70 mm (new flame-spread

## 4. Conclusions

The interaction between flame-spread and droplet motion was investigated under normal gravity conditions. Initial spacings between the fourth fixed-droplet, the first movable droplet and the second movable droplet were varied. Five flame-spread patterns were observed.

## Acknowledgments

This study was carried out as a part of “Research Working Group Activity of Space Environment Science” supported by ISAS-JAXA.

## References

1) Hiroshi NOMURA, Masato MIKAMI, Masao KIKUCHI, Daniel L. DIETRICH, Proceedings of the 27th Journal of the Japan Society of Microgravity Application, 2013

28A07

# 大気球を利用した微小重力燃焼実験の実施結果について

○菊池政雄，石川毅彦（JAXA），山本信（IHI 検査計測），澤井秀次郎，丸祐介，橋本樹明，
坂井真一郎，坂東信尚，清水成人，小林弘明，吉光徹雄，菅勇志，水島隆成（JAXA），
福山誠二郎（AES），岡田純平，依田眞一，福家英之，梯友哉（JAXA）

# Result of Microgravity Combustion Experiment by Using Balloon Operated Vehicle

○Masao KIKUCHI, Takehiko ISHIKAWA (JAXA) , Shin YAMAMOTO (IIC), Shujiro SAWAI, Yusuke MARU,
Tatsuaki HASHIMOTO, Shinichiro SAKAI, Nobutaka BANDO, Shigehito SHIMIZU, Hiroaki KOBAYASHI,
Tetsuo YOSHIMITSU, Yuji KAN, Takanari MIZUSHIMA (JAXA), Seijiro FUKUYAMA (AES),
Junpei OKADA, Shinichi YODA, Hideyuki FUKE, Yuya KAKEHASHI (JAXA)

## 1. Introduction

The usefulness of the high-altitude balloon operated vehicle as a microgravity experiment method with high quality microgravity level was demonstrated by Hashimoto et al.[1-4]. It was shown that the experimental system could provide low-gravity environment in the order of $10^{-4}$ G for around 30 s by drag-free control of the payload, which is accommodated inside the outer structure of the free falling vehicle. However, maximum payload size was very limited in previous system.

In order to enlarge the allowable payload size with sustaining microgravity level, development of new drag-free control method was performed by Ishikawa et al.[5]. For technical demonstration of the new system, a flight experiment using the high-altitude balloon was planned. Preparation effort of the flight experiment at the JAXA's Taiki Aerospace Research Field (TARF) , located in the Taiki town in Hokkaido, was performed in the summer of 2012 at first. However, the flight experiment was not achieved due to bad weather condition in 2012. Although flight experiment was also tried in the spring of 2013 and 2014, it resulted in postponement of the experiment due to bad weather conditions. Finally, the flight experiment was performed in the summer of 2014 as the 4th trial at the TARF.

This paper briefly reports the outline of the experiment and its result.

## 2. Overview of the Experiment

The primary objective of the flight experiment is demonstration and verification of the new drag-free experiment system. As described detail in later, the new system was designed to accommodate a payload whose size is as large as that of European TEXUS sounding rocket. Since experimental apparatus called DCU (Droplet Array Combustion Unit), employed for the droplet array combustion experiment by TEXUS 46 in 2009[6], was available, it was employed for the payload of this flight experiment. For the flight experiment, engineering model (EM) of the DCU was modified so that it meets flight operation by the balloon operated vehicle. It was also intended to obtain scientific data on flame spread along a linear fuel droplet array with pre-vaporization in microgravity[7].

**Fig. 1** shows schematic concept of the combustion experiment. Same as previous TEXUS rocket experiment, observation of flame spread phenomena along n-decane droplet array in 500 K air was planned in the current experiment. In the TEXUS rocket experiment, flame spread with relatively large degree of pre-vaporization was observed 3 times by varying pre-vaporization time during 6 minutes microgravity[6]. On the other hand, 1 time observation of flame spread with relatively small degree of pre-vaporization during about 30 s microgravity was intended in the current experiment. It was expected that data obtained by the balloon experiment would fill the gap between those by short duration drop tower/shaft experiments and by longer duration TEXUS rocket experiments.

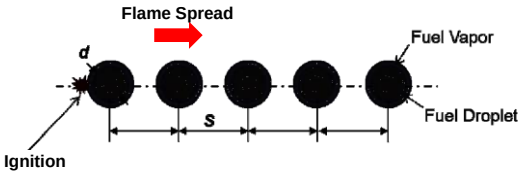


**Fig. 1** Schematic concept of the combustion experiment

## 3. Experimental System

The differences of drag-free control methods in previous and current system are indicated in **Fig. 2**. In previous system (a), the three dimensional (3D) relative position of the inner capsule (payload of the microgravity experiment) was measured from outer capsule, and the cold gas jets in the outer capsule produced forces to cancel the disturbances and kept the distance between the inner and outer capsule constant. Although the 3D control method realized high quality microgravity environment during free falling of the balloon operated vehicle, it was almost impossible to accommodate larger size payload.

In the current system (c), a one dimensional (1D) drag-free control system using a linear slider mechanism was adopted. The payload and the outer capsule (balloon operated vehicle) is mechanically connected by a linear slider. When the vertical distance between the payload and inner wall of the vehicle decreases by drag force to the vehicle, longitudinal cold gas jets

thrusters at the rear end of the vehicle are activated so that they cancel disturbances and maintain appropriate distance between the payload and the inner wall of the vehicle. Better low gravity environment by this system was expected than the system without any drag-free control system (b).

As a result, allowable payload size was enlarged to 400 mm in diameter and 600 mm in height, from spherical shape in 280 mm diameter by previous system.

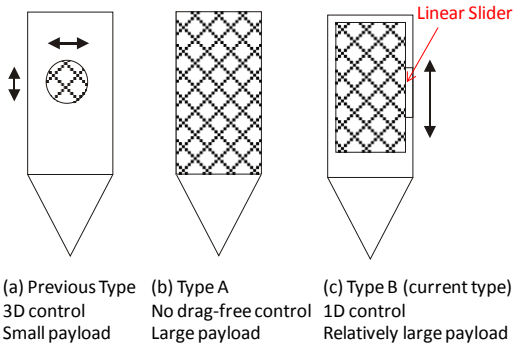


**Fig. 2** Comparison of drag-free control methods of the payload

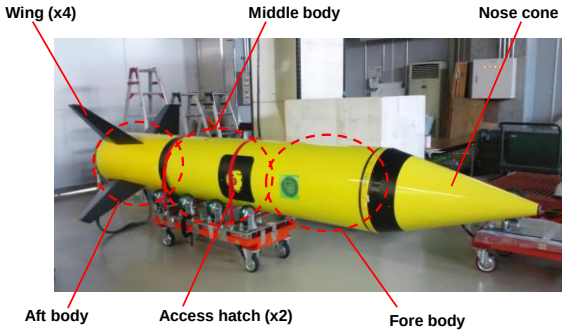


**Fig. 3** Appearance of the balloon operated vehicle

**Fig. 3** shows a photo of the balloon operated vehicle on the ground. The shape of the vehicle (outer capsule for the payload) is almost identical to the previous system. Total length of the vehicle is about 4.1 m and outer diameter of the body is about 0.6 m. The weight of the vehicle including the payload described in detail later is about 310 kg. The vehicle consists of nose cone, fore body, middle body, and aft body with 4 wings. The fore body and the middle body accommodate system devices of the vehicle as well as the payload. The aft body accommodates parachute of the vehicle and cold gas jets thrusters. The fore body and the middle body are airtight structures, so that inner pressure is kept at atmospheric pressure (about 1 atm) even at higher altitude. Also, the structures protect inner devices from sea water after splashdown in the sea.

**Fig. 4** shows a photo of the modified EM of the DCU, employed as the payload of the current experiment. The weight of the payload is about 50 kg. Although the control device and batteries for the payload were provided by the rocket side in the TEXUS experiment, whole system shall be prepared by the payload itself in the current experiment by the balloon operated vehicle. Therefore, control devices and batteries were additionally installed in the experimental apparatus. Also, observation devices including a high-speed video camera were replaced to new one.

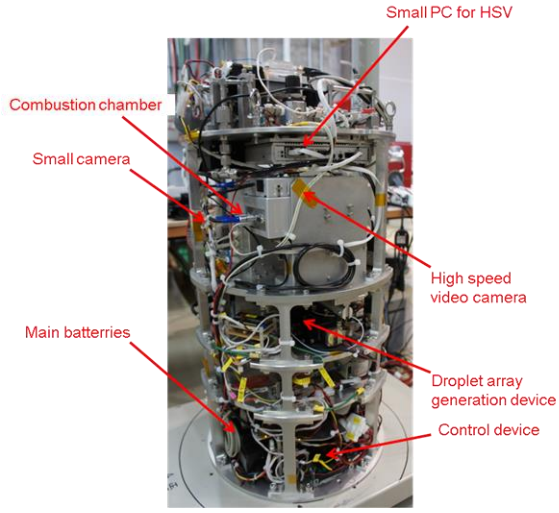


**Fig. 4** Photo of the modified EM of the DCU

The whole experimental system for microgravity experiment by the balloon operated vehicle consists of the high altitude balloon system, the balloon operated vehicle, and the payload inside the vehicle. Configuration of these systems is schematically shown in **Fig. 5**. It is possible to lift scientific payloads with 700 kg to an altitude of 40 km, by the high

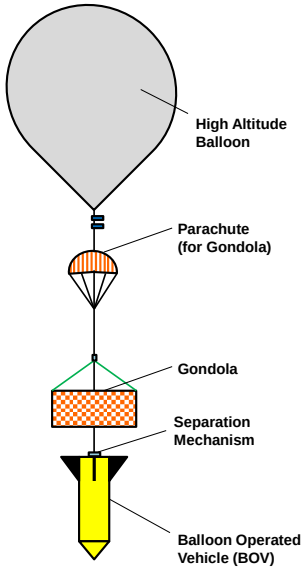


**Fig. 5** Schematic of the whole configuration of the balloon experiment system

altitude balloon filled with helium gas. The balloon operated vehicle is lifted up by the balloon via the gondola. Control devices, electrical batteries, communication devices, and other system devices for the balloon system are accommodated in the gondola. Maximum height of these systems is beyond 150 m.

## 4. Result of the Experiment

Final ground operation at the TARF for the flight experiment was started at about 23:30 on August 21. Power system, control system, and communication system of the vehicle were turned on. Also, every access hatches of the vehicle body were closed. Confirmations on transmission and reception conditions of the telemetry signals and telecommands were performed between the vehicle and the ground system. After every preparation of the vehicle was completed, injection of helium gas to the high altitude balloon was started at around 03:00 on August 22. Finally, the balloon with the vehicle was released to air at around 04:30. Photos of the balloon and the vehicle during final preparation phase are shown in **Fig. 6** and **Fig. 7**. Also, sequential photos of the vehicle at the moment of the balloon release are shown in **Fig. 8**.

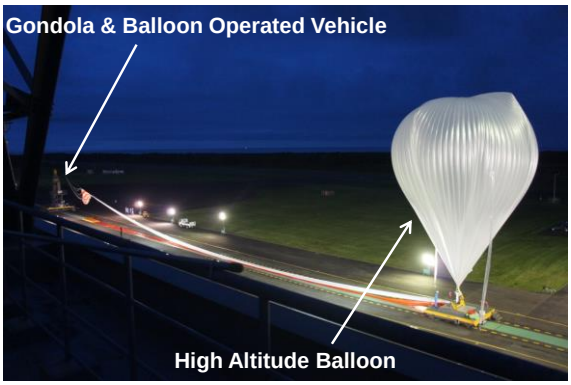


**Fig. 6** Whole view of the high altitude balloon, the gondola and the balloon operated vehicle before the release

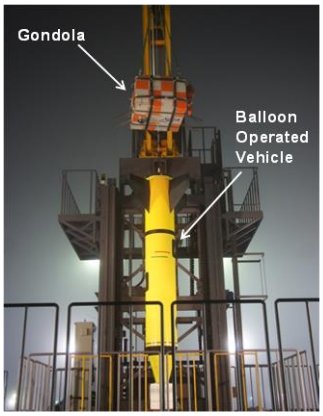


**Fig. 7** Photo of the gondola and the balloon operated vehicle before the release

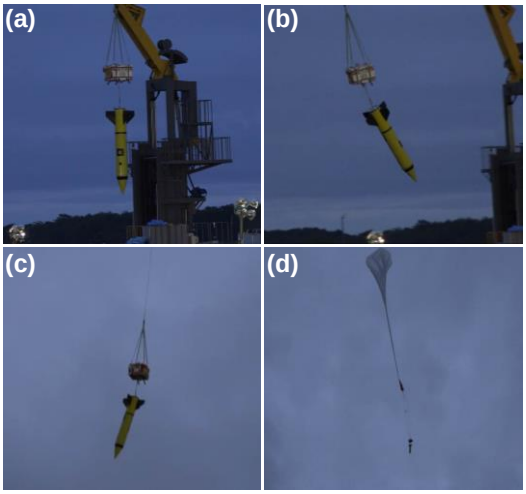


**Fig. 8** Sequential photos of the balloon operated vehicle after the release of the balloon

During ascent of the balloon, several telecommands for experiment preparation were sent to the vehicle from the ground. Heating of the combustion chamber of the payload was started at around 5:50. Temperature inside the combustion chamber increased to 500 K within 45 minutes, same as nominal ground test. 5 minutes prior to the release of the vehicle from the gondola, automatic timer sequence of the experiment procedures was started. The vehicle was released from the gondola at 7:11. Sequential photos of the vehicle after the release, obtained by video camera at the gondola, are shown in **Fig. 9**.

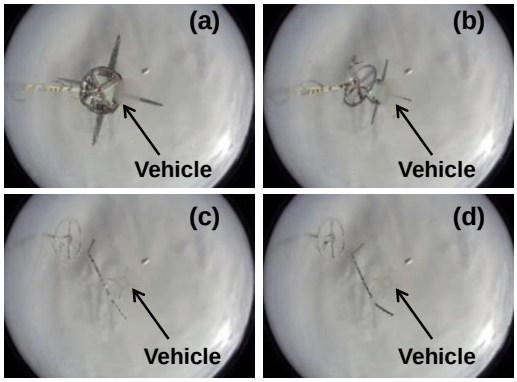


**Fig. 9** Sequential photos of the vehicle after the release from the gondola

During free fall of the vehicle, experiment sequences of the payload such as generation of n-decane droplet array on the array holder, insert of the array holder into the combustion chamber, activation of igniter after 3 s pre-vaporization time in the chamber, recording of high-speed video camera and backlit camera et al. were automatically performed. About 35 s after the release of the vehicle, pilot parachute at the rear end of the

vehicle was deployed and free fall of the vehicle was completed. Also, about 320 s after the release of the vehicle, main parachute was deployed from the vehicle. The vehicle splashed down the sea at around 7:27. Finally, the vehicle in addition to the gondola and balloon were retrieved by ships.

After the retrieval of the vehicle, experimental data including high-speed video camera and backlit camera were normally retrieved. Also, measurement data of ambient condition of the payload inside the vehicle, including temperature, humidity as well as microgravity level, were successfully retrieved. **Fig.10** shows the history of the measured data of the payload acceleration in 3-axis direction during free falling of the vehicle. Z-axis means the longitudinal direction along the vehicle body, and X and Y-axis mean the lateral directions. In **Fig. 10**, the free falling of the vehicle starts at around 8 s of the horizontal axis. By 22 s of the horizontal axis (14 s after the start of free falling), some spike-like disturbances of gravity level are indicated for all 3-axis. These disturbances are attributed to the motion of experimental devices of the payload, such as movement of the droplet generation device, opening the shutter of the combustion chamber, and insert of the array holder into the combustion chamber. After this phase, relatively calm gravity level is maintained by around 33 s of the horizontal axis. The timing of igniter activation for droplet ignition corresponds to this stable gravity duration. After 33 s, spike-like disturbances appear again due to motion of experimental devices, followed by large disturbances at around 40 s due to deployment of the parachute of the vehicle. Apart from the disturbances induced by the motion of experimental devices, it was confirmed that the balloon operated vehicle successfully provided good low gravity condition for more than 20 s.

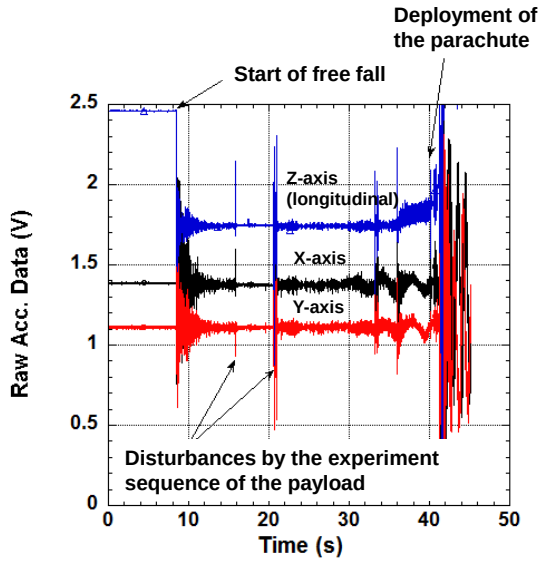


**Fig. 10** Measurement data of the payload acceleration in 3-axis direction during free falling

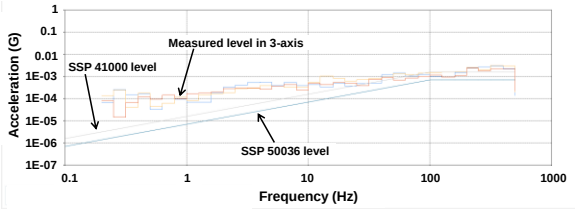


**Fig. 11** Comparison of the measured gravity level in 3-axis with microgravity level of the ISS

**Fig. 11** shows the comparison of the measured gravity level in 3-axis during 30 s after the start of free falling, with required microgravity level of the ISS. According to the result, the gravity level of the payload is less than $10^{-3}$ G in low frequency region (less than 100 Hz), though it exceeds $10^{-3}$ G in high frequency region (more than 100 Hz). It means gravity level achieved by the new drag free system is still high level even the accommodated payload size is significantly enlarged. In addition, it should be noted that gravity level in low frequency region was lower than that of the ISS.

As for the combustion experiment by the payload, activation of the igniter (Fe-Cr wire) was confirmed by the obtained video image at nominal timing. However, ignition of the n-decane droplet was not occurred. **Fig. 12** shows the igniter which is glowing by electric current during the experiment. The brightness of the igniter was lower than that observed in the ground tests. Also, the time length of glowing was shorter than that measured in the tests. It could be possible that dew condensation on the igniter surface due to temperature variation during the flight experiment may cause this trouble, though detail investigation is underway, at present.

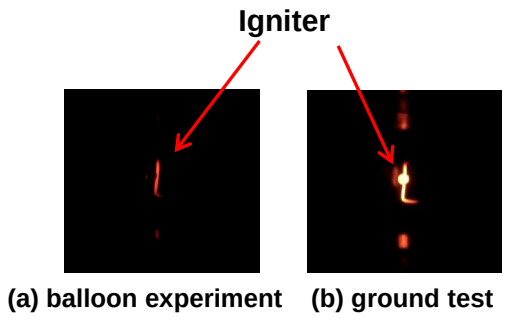


**Fig. 12** Comparison of the glowing igniter

## 5. Summary

The flight experiment by the balloon operated vehicle was performed at the JAXA's Taiki Aerospace Research Field (TARF) in the summer of 2014. The primary objective of the flight experiment was demonstration and verification of the new drag-free experiment system for microgravity experiment. Also, combustion experiment on flame spread of n-decane droplet

array was intended. The whole flight experiment including the retrieval of the vehicle was successfully performed. According to the obtained data, it was confirmed that the vehicle with new drag-free system successfully realized low-gravity environment in the order of $10^{-3}$ G for more than 20 s. Regarding the combustion experiment, ignition of the fuel droplet was not occurred due to insufficient glowing of the igniter.

## References


1) Hashimoto, T., Sawai, S., Sakai, S., Bando, N., Kobayashi, H., Ishikawa, T., Inatomi, Y., Fujita, K., Yoshimitsu, T., Saito, Y., and Fuke, H.: *J. Jpn. Soc. Microgravity Appl.*, **26**, (2009), pp. 9-14.

2) Ishikawa, T., Inatomi, Y., Hashimoto, T., Sawai, S., Saito, Y., Yoshimitsu, T., Sakai, S., Kobayashi, H., Fujita, K., Bando, N., Goto, M.: *J. Jpn. Soc. Microgravity Appl.*, **25**, (2008), pp. 3-10.

3) Sawai, S., Hashimoto, T., Sakai, S., Bando, N., Kobayashi, H., Yoshimitsu, T., Ishikawa, T., Inatomi, Y., Fuke, H., Kamata, Y., Hoshino, S., Tajima, K., Kadooka, S., Uehara, S., Kojima, T., Ueno, S., Miyaji, K., Tsuboi, N., Hiraki, K., Suzuki, K., Matsushima, K., and Nakata, T.: *JSASS* **56**, (2008), pp.339-346.

4) Ishikawa, T., Hashimoto, T., Sawai, S., Saito, Y., Inatomi, Y., Yoshimitsu, T., Sakai, S., Kobayashi, H., Fujita, K., and Bando, N.: *Transaction of JSASS Space Tech. Japan* **7** (2009), pp.29-33.

5) Ishikawa, T., Kikuchi, M., Yamamoto, S., Sawai, S., Maru, Y., Hashimoto, T., Sakai, S., Bando, N., Shimizu, S., Kobayashi, H., Yoshimitsu, T., Kan, Y., Tazaki, A., Fukuyama, S., Okada, J., Yoda, S., Fuke, H., and Kakehashi, Y.: *Proc. FY24 Balloon Symposium (in Japanese)*, 2012, isas-12-sbs-023.

6) Kikuchi, M., Yamamoto, S., Mikami, M., Nomura, H., Moriue, O., and Umemura, A.: *Proc. 49th Combustion Symposium (Japanese)*, 2011, pp.108-109.

7) Kikuchi, M., Ishikawa, T., Yamamoto, S., Maru Y., Bando, N., Kan, Y., Tazaki, A., Fukuyama, S., Okada, J., and Fuke, H.: *Transaction of JSASS Space Tech. Japan* **12** (2014), to be published.